Supporting information

# DNA compaction and dynamic observation in a nanopore gated sub-attoliter silicon nanocavity

Shuangshuang Zeng[1, 2], Mauro Chinappi[3], Fabio Cecconi[4, 5], Theo Odijk[6], Zhen Zhang[1, *]

1. *Division of Solid-State Electronics, Department of Electrical Engineering, Uppsala University, SE-751 03 Uppsala, Sweden*
2. *Present address: Institute for Chemical and Bioengineering, ETH Zürich, 8093 Zürich, Switzerland*
3. *Dipartimento di Ingegneria Industriale, Università di Roma Tor Vergata, Via del Politecnico 1, 00133 Roma, Italia*
4. *CNR-Istituto dei Sistemi Complessi, Via dei Taurini 19, 00185 Roma, Italia*
5. *INFN, Unità di Roma 1, 00185, Roma, Italia*
6. *Lorentz Institute for Theoretical Physics, University of Leiden, Niels Bohrweg 2, 2333 CA Leiden, The Netherlands*

** Corresponding authors: zhen.zhang@angstrom.uu.se*

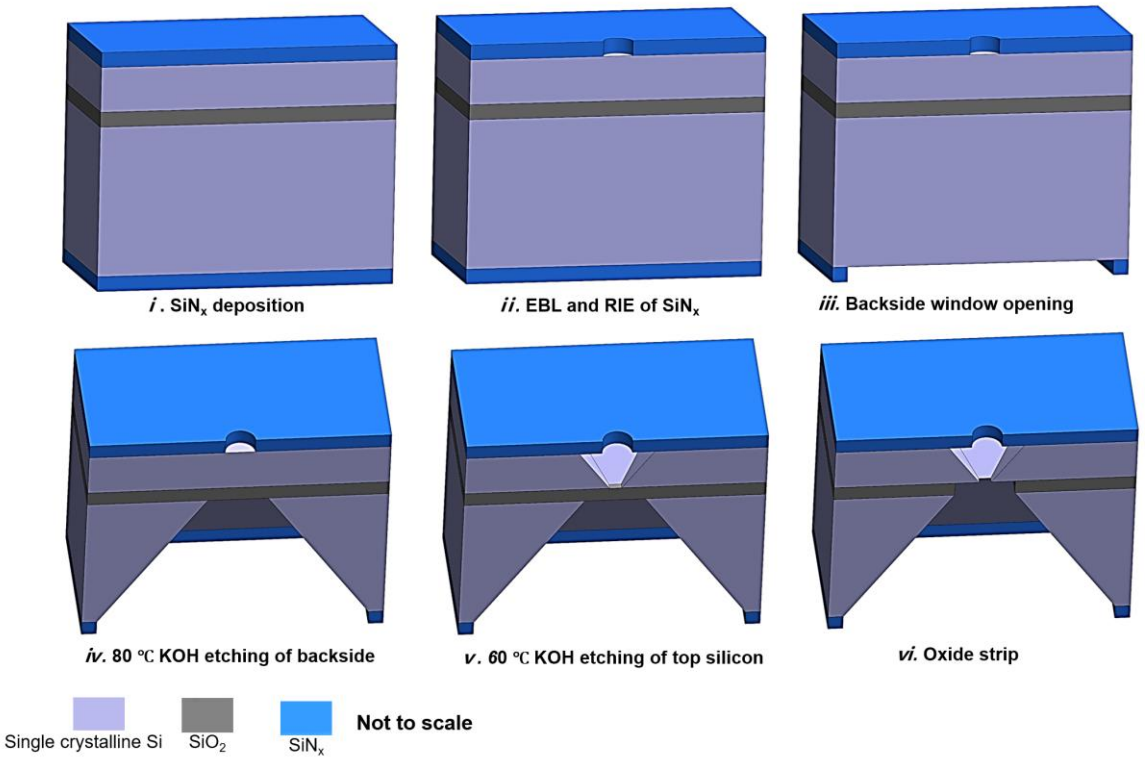


Figure S1. Schematic illustration of the nanopore gated nanocavity fabrication process. (a) $SiN_x$ deposition on SOI wafer by means of low-pressure chemical vapor deposition (*i*), electron beam lithography (EBL) and reactive ion etching (RIE) patterning in $SiN_x$ layer (*ii*), backside window opening using photolithography followed by RIE (*iii*), silicon (Si) etching in the bulk substrate by combing deep RIE and 80 ℃ KOH wet etching (*iv*), top Si etching in 60 ℃ KOH solution (*v*) and buried oxide removal by buffered HF (*vi*).

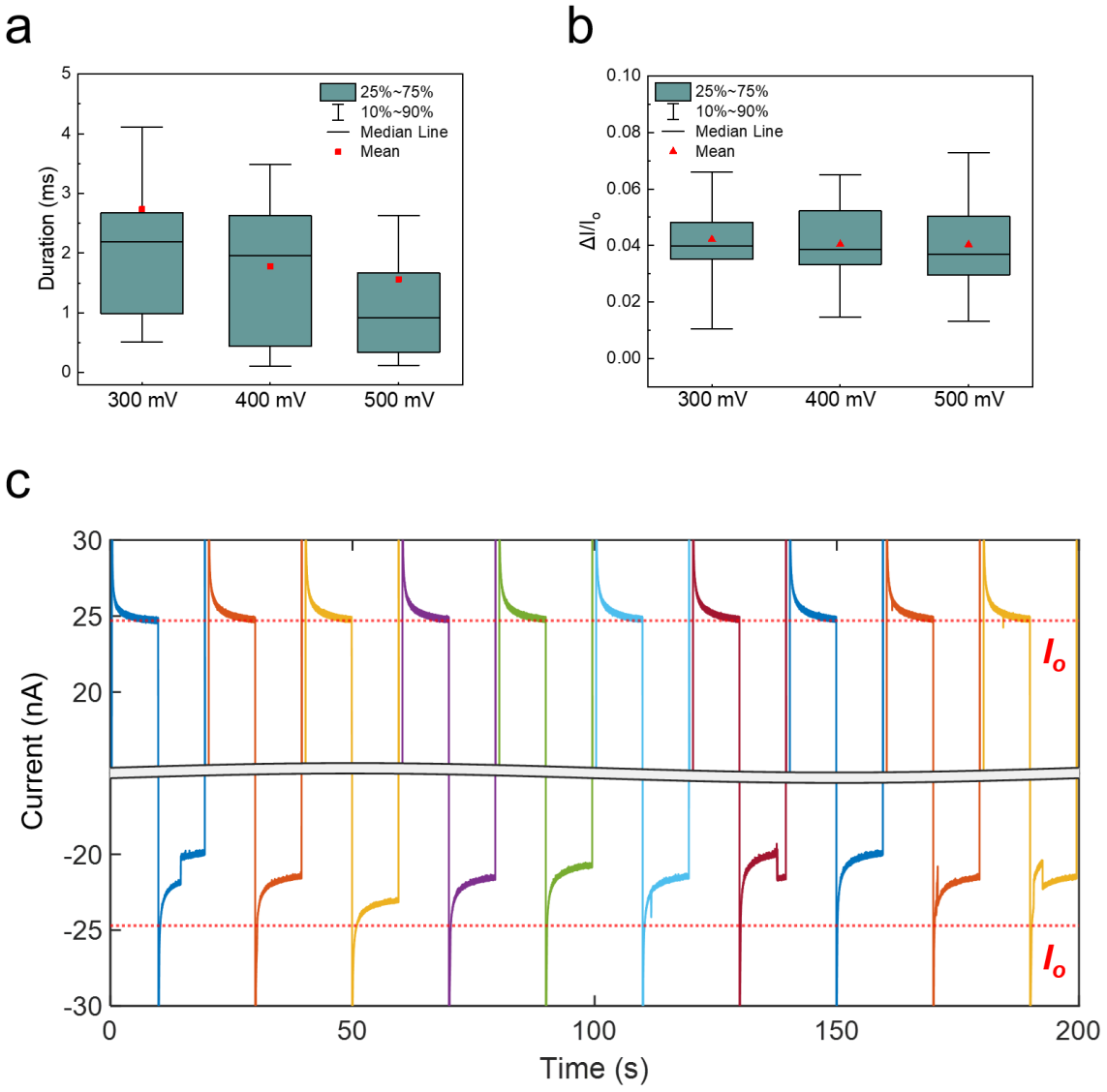


Figure S2. Analysis of translocation events of 20 kb DNA through Device 1 at different positive applied voltage and ionic current measured by switching the applied bias between 400 mV and -400 mV. (a) Box plot of duration of translocation event at 300 mV, 400 mV and 500 mV, respectively. (b) Box plot of relative amplitude of translocation event ( $\Delta I/I_o$) at 300 mV, 400 mV and 500 mV, respectively. (c) Ionic current measured by switching the applied bias between 400 mV and -400 mV (remain 10 s at each bias polarity) for 10 times. The ionic current at -400 mV is always smaller than the open pore current $I_o$ (marked by the red dash line) and shows strong fluctuations, while the baseline current at 400 mV always remains at the same level of $I_o$.

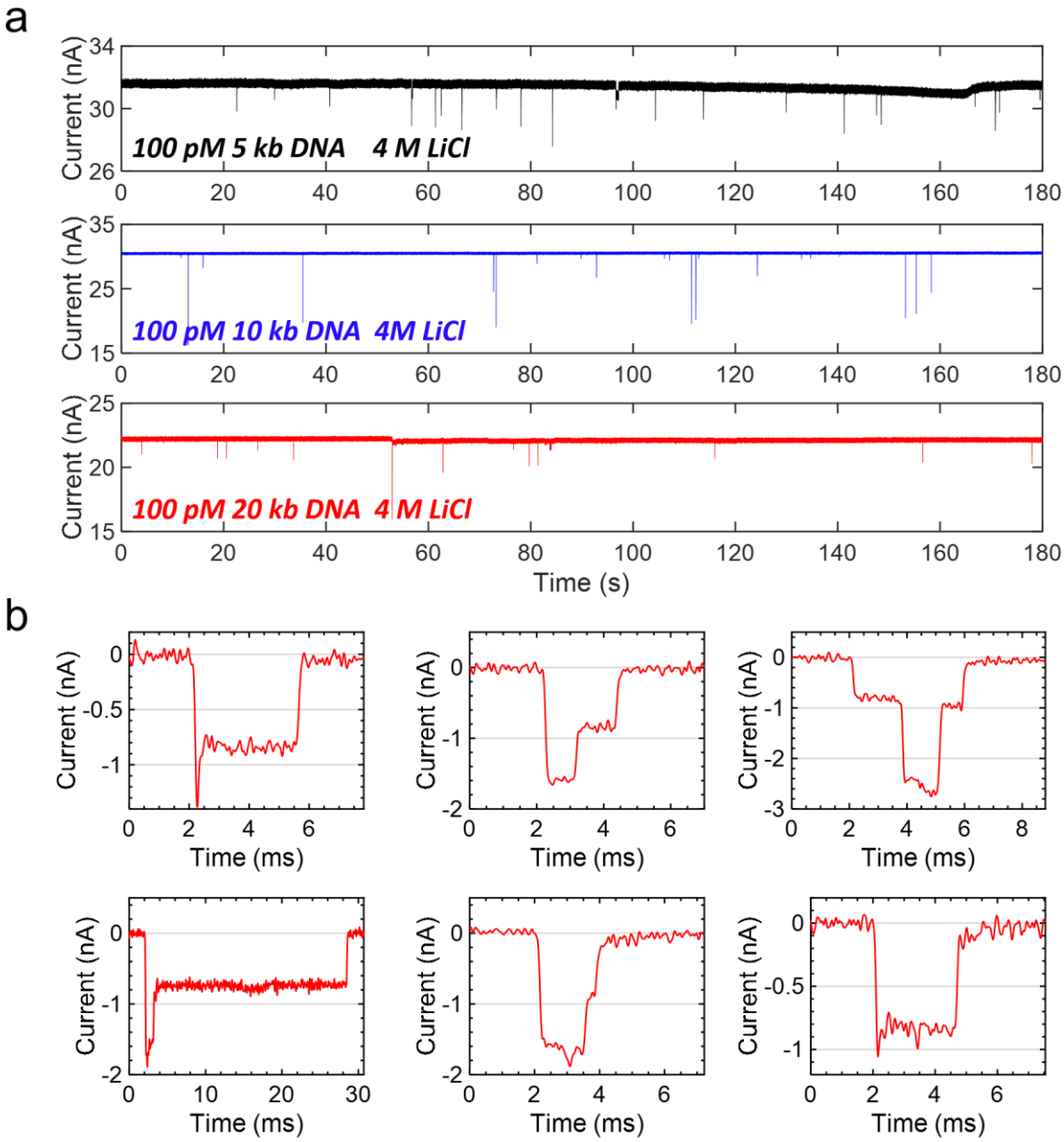


Figure S3. Ionic current measurements of 100 pM DNA through Device 1 with different DNA lengths in 4 M LiCl at 400 mV. (a) Ionic current traces for the measurements with different DNA lengths. It is worthy of noting that after using the same device for measurements of multiple times, the Si pore size became enlarged, as evidenced by the different baseline current. This can be caused by slight etching of Si in such high concentration electrolyte (4M LiCl). (b) Exemplified view of typical translocation events for 20 kb DNA.

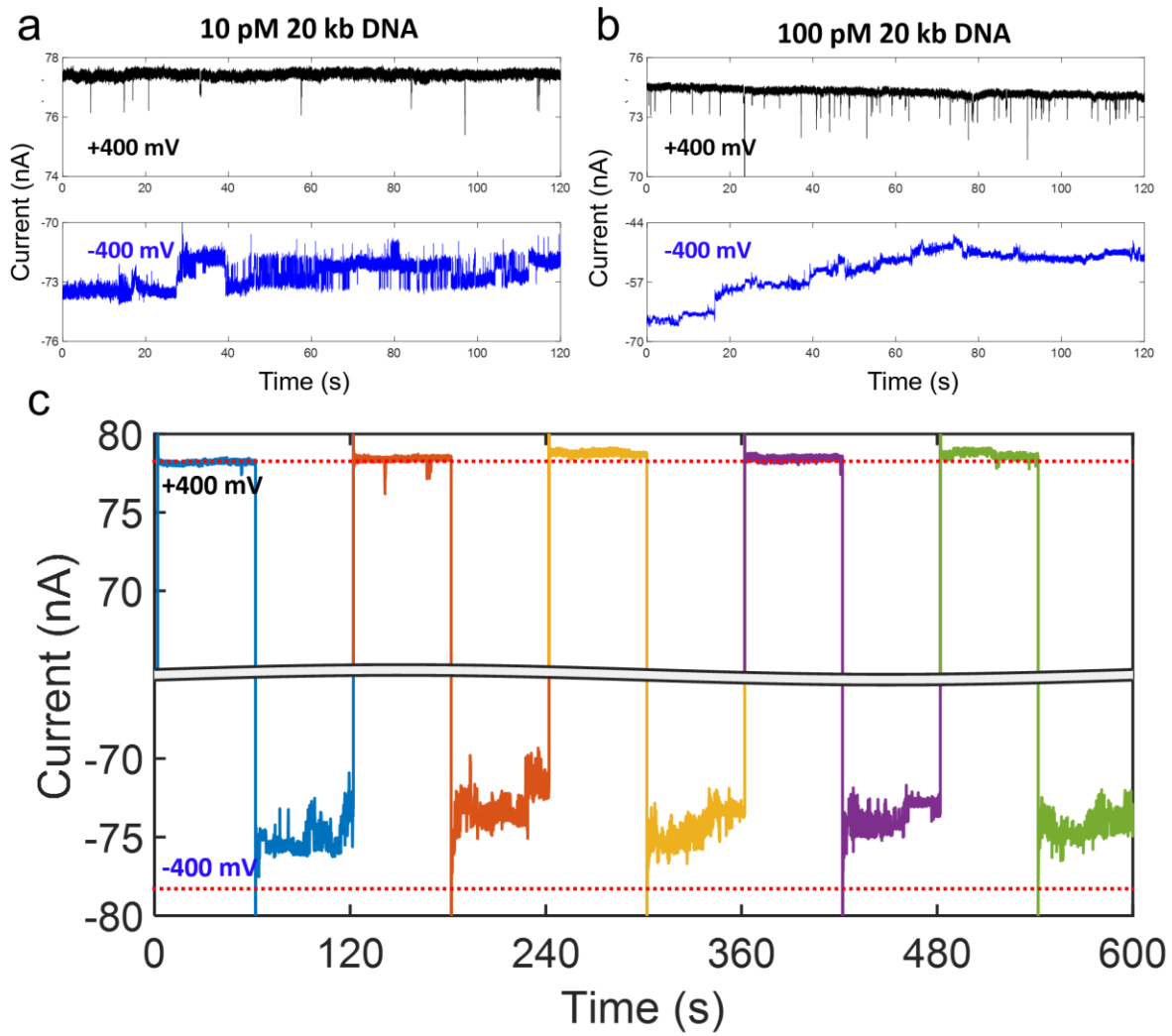


Figure S4. Ionic current measurements of 20 kb DNA in 4 M LiCl at 400 mV and -400 mV (a) Ionic current trace with 10 pM DNA. The capture at 400 mV is around 0.09 $s^{-1}$. (b) Ionic current trace with 100 pM DNA using the same device. The capture at 400 mV is around 0.44 $s^{-1}$. A clear dependence of the capture rate on the DNA concentration is seen. (c) Ionic current traces with 10 pM DNA by reversing the applied bias from 400 mV to -400 mV (remain 60 s at each bias polarity) for 5 times.

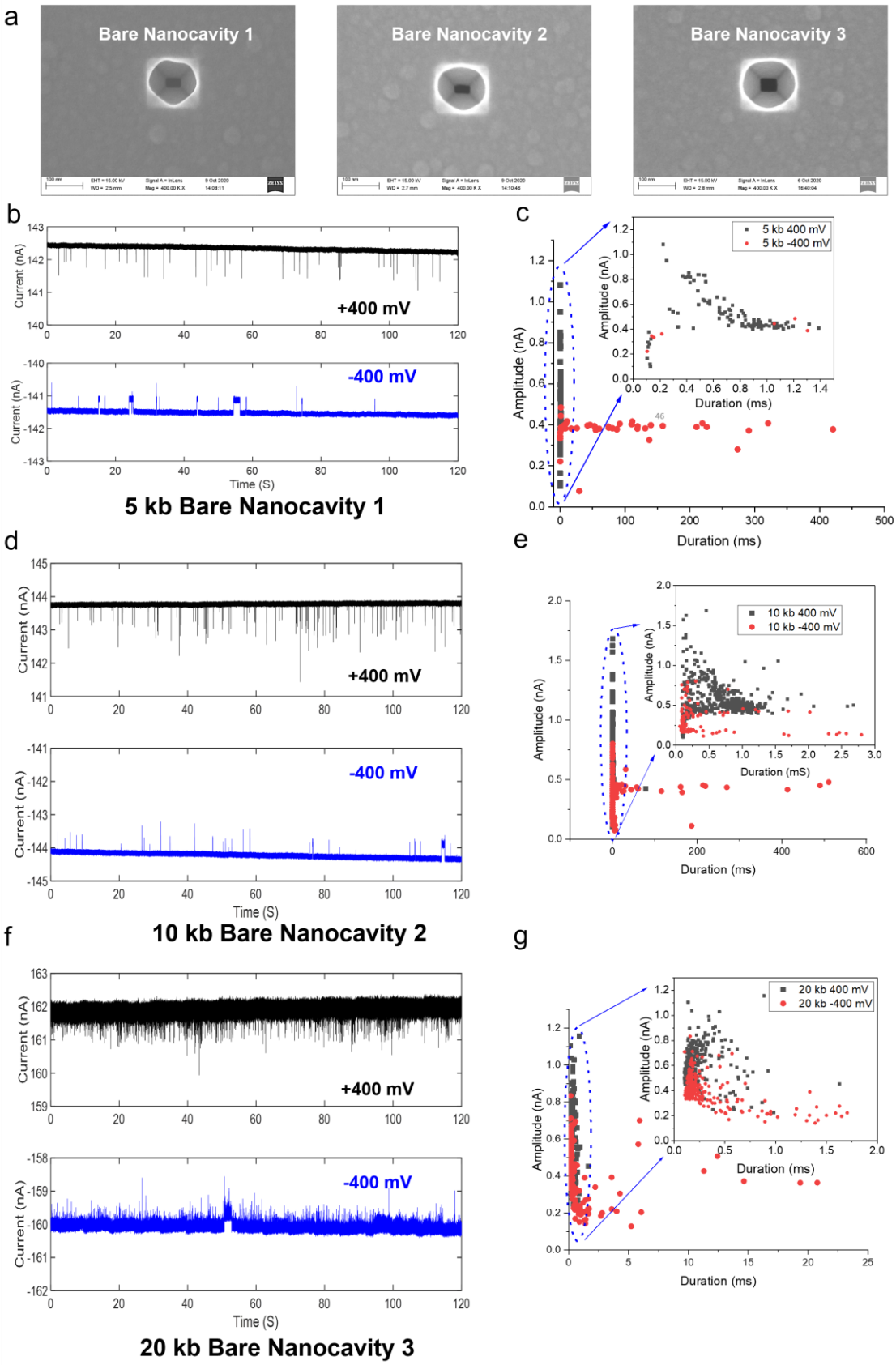


Figure S5. Ionic current measurements of 100 pM DNA translocation through bare Si nanocavities (no top $SiN_x$ nanopore) with different DNA lengths in 4 M LiCl at 400 mV and -400 mV, respectively. (a)

SEM iamges of three different bare Si nanocavities. (b, d, f) Ionic current traces of 5 kb, 10 kb and 20 kb DNA translocation events. (c, e, g) Scatter plots of 5 kb, 10 kb and 20 kb DNA translocation events.

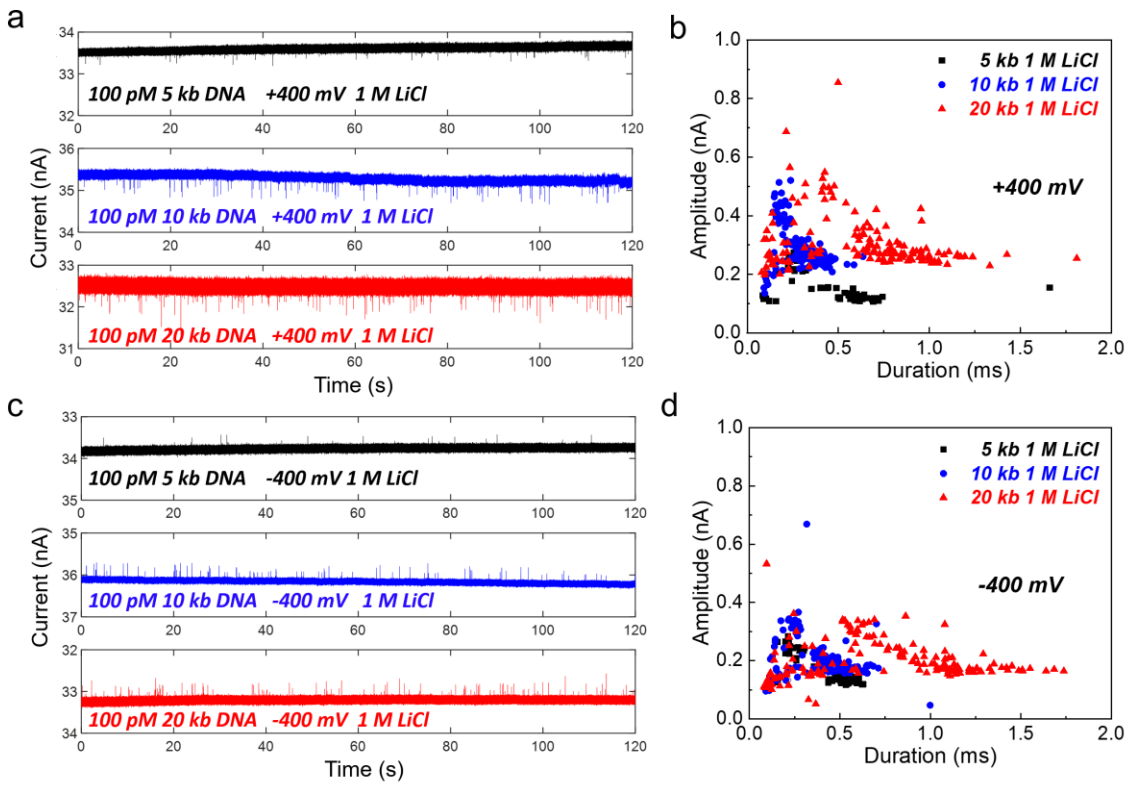


Figure S6. Ionic current measurements and scatter plot of DNA translocation events with different DNA lengths in 1 M LiCl passing Device 2 at +400 mV and -400 mV, respectively. (a) Ionic current traces of 5 kb, 10 kb and 20 kb DNA translocation through Device 2 at +400 mV. (b) Distribution of the amplitude and duration of the translocation events in (a). (c) Ionic current traces of 5 kb, 10 kb and 20 kb DNA translocation through Device 2 at -400 mV. (d) Distribution of amplitude and duration of the translocation events in Figure (c).

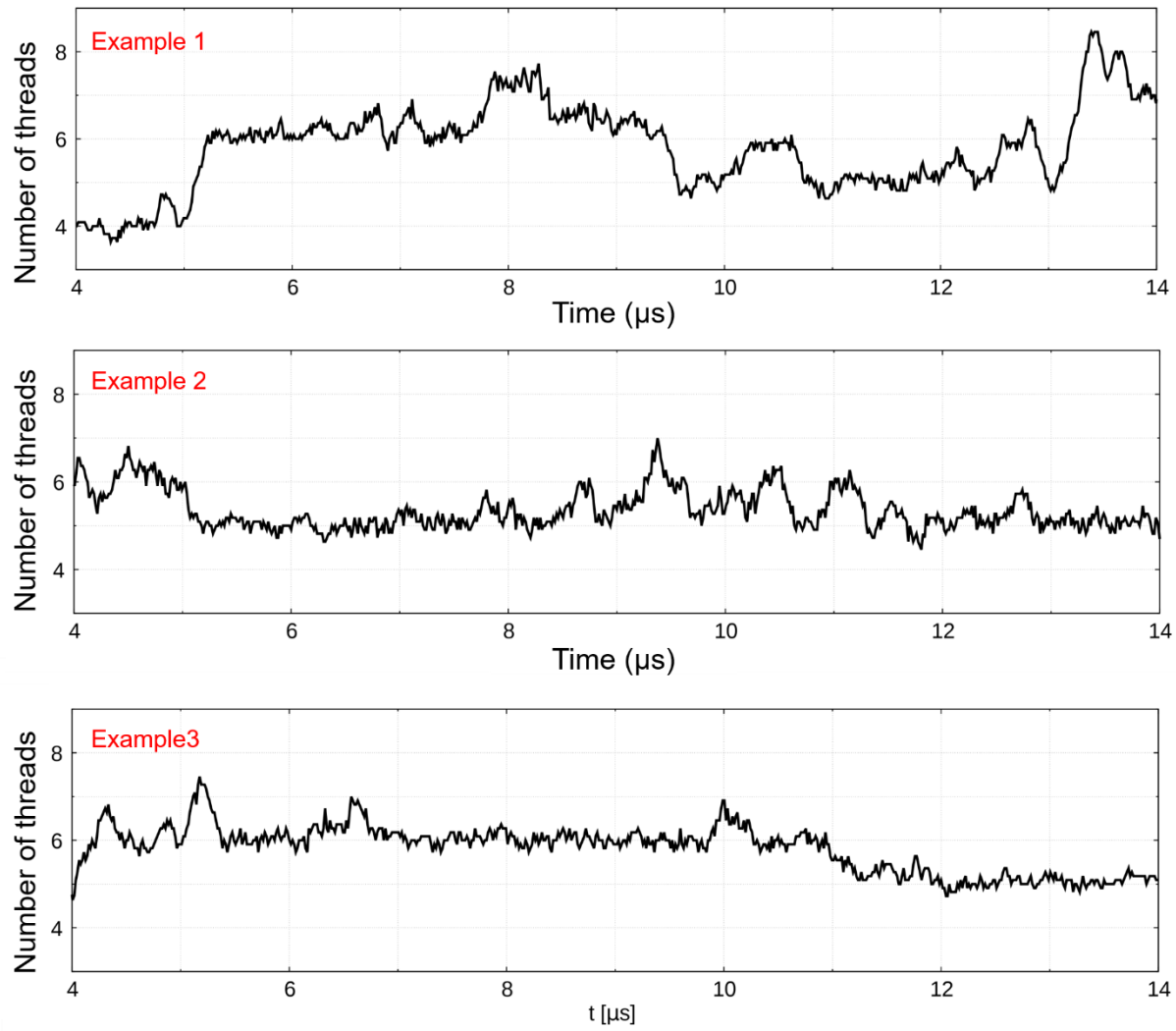


Figure S7. Examples of the time evolution of the number of DNA threads in the Si pore constriction after DNA compaction in a nanocavity device, from Brownian simulations. Data refers to different simulation replicas. The signal is obtained as a running average over a window of 1/100 of the entire simulation and, therefore, it is not an integer.

## SUPPLEMENTARY METHODS S1. SIMULATION SET-UP

We used a coarse-grained Brownian approach to model the dynamics of the dsDNA inside the nanopore under the action of an voltage. The DNA is described as a chain of beads and springs plus additional potentials to enforce the prescribed persistence length $\ell_p = 50$ nm and to take into account excluded volume among different DNA filaments. Electrophoresis, electroosmosis and pore confinement are included as external actions on the polymer beads. Electric and velocity fields were pre-calculated solving a stationary Navier-Stokes Poisson-Nernst-Planck (NS-PNP) system [1, 2]. In the following, the description of each modelling ingredient is reported.

**Coarse grained model of DNA.** The coarse-grained model of DNA consists in an almost inextensible polymer chain of $N$ beads of mass $m$, charge $q$ and position $\mathbf{r}_i$ with a persistence length, $\ell_p$, (worm like chain, WLC). Therefore the potential energy describing the system is

$$U(\mathbf{r}_1, \ldots, \mathbf{r}_N) = \frac{K_h}{2b^2} \sum_{i=1}^{N-1} (|\mathbf{r}_{i+1} - \mathbf{r}_i| - b)^2 - \frac{k_B T \ell_p}{b^3} \sum_{i=2}^{N-1} (\mathbf{r}_{i+1} - \mathbf{r}_i) \cdot (\mathbf{r}_i - \mathbf{r}_{i-1}) + U_{NB}\,, \quad (1)$$

where the first term is the sum of stiff harmonic potentials such that each bond length can only perform negligible fluctuations around its equilibrium value, $|\mathbf{r}_{i+1} - \mathbf{r}_i| \simeq b$ (almost inextensible condition). The second term represents the penalty that the chain has to pay upon bending, it enforces a chain in the bulk to maintain, on average, a persistence length, $\ell_p$. $T$ is the temperature while $k_B$ is the Boltzmann constant. Note that, in general, the bending potential is equivalently expressed as $k_B T \ell_p b^{-1} \sum_{i=2}^{N-1} (\mathbf{n}_{i+1} \cdot \mathbf{n}_i)$, where $\mathbf{n}_{i+1}$ is the unit vector from bead $i$ and $i+1$ [3]. However, since our polymer is almost inextensible, we preferred the expression (1) that is computationally less expensive. $U_{NB}$ refers to non-bonded interactions that are modelled as a Weeks-Chandler-Anderson (WCA) potential, i.e. Lennard-Jones truncated at its minimum, acting among all the beads with the exception of first and second neighbours. Electrostatic repulsion is not included in the non-bonded interaction since experiments are run at high salt concentration (typically $4M$) resulting in an almost complete screening of the electrostatic interaction on the scale of our coarse-graining.

We simulate the action of the external field as an electrosmotic velocity and an electrophoretic force. Moreover, interaction with impenetrable solid walls of the pore is considered. Accordingly, the motion of each bead is governed by the Langevin system

$$\begin{aligned} \dot{\mathbf{r}}_i &= \mathbf{v}_i \\ m\dot{\mathbf{v}}_i &= -\gamma(\mathbf{v}_i - \mathbf{v_f}) - \nabla_{\mathbf{r}_i} U + q\mathbf{E} + \mathbf{G}_i + \mathbf{R}_i\,. \end{aligned} \quad (2)$$

The term $-\gamma(\mathbf{v}_i - \mathbf{v_f})$, with $\mathbf{v_f}(\mathbf{r}_i, t)$ the velocity of the fluid, is the drag exerted on the polymer by the electroosmotic flow of the solvent. The term $-\nabla_{\mathbf{r}_i} U$ represents the internal forces of the chain on the $i$-th bead, see Eq. (1). The term $q\mathbf{E}$, with $\mathbf{E}(\mathbf{r}_i, t)$ the external electric field, is the electrophoretic force and $\mathbf{G}_i$ indicates all the other external forces mimicking the impenetrability of the membrane and the pore walls. Finally, $\mathbf{R}_i$ denotes a random force, accounting for the collisions with the solvent, and fulfilling the fluctuation dissipation relation $\langle \mathbf{R}_i \rangle = 0$ and $\langle R_{\mu,i}(t) R_{\nu,j}(0) \rangle = 2k_B T \gamma \delta_{\mu,\nu} \delta_{i,j} \delta(t)$, with $\mu, \nu = \{x, y, z\}$. Eqs.(2) are numerically integrated via a leap-frog algorithm [4], with constant integration time-step $\delta t = 0.4$ ps for all the runs.

**Electrohydrodynamics simulations.** The Langevin model in Eqs.(2) is completed when suitable expression for the electroosmotic velocity $\mathbf{v_f}(\mathbf{r}, t)$, the electric field $\mathbf{E}(\mathbf{r}, t)$ and wall repulsion force $\mathbf{G}(\mathbf{r}, t)$ are provided. For pores whose narrowest section is of the order of a nanometer and/or whose solvent-exposed surface presents a complex shape/charge nanoscale pattern (e.g. biological pores), reliable expressions of $\mathbf{v}_f(\mathbf{r}, t)$, $\mathbf{E}(\mathbf{r}, t)$ and $\mathbf{G}(\mathbf{r}, t)$ may be obtained with atomistic approaches such as all-atoms molecular dynamics simulations (MD), see e.g. [5–7]. For larger pores, continuum models are expected to provide reliable approximation of electrohydrodynamics [8, 9]. When the nanopores has a simple shape, such as a cylinder, a combination of ideal electroosmotic flow solution in the pore and hemispherical models for the entrance regions can provide a reliable first approximation of the continuum electrohydrodynamics [1, 10–12]. However, since the geometry of the pore employed in this study too complicated for a theoretical approach, we opted for a numerical solution of the electrohydrodynamics.

We solved standard Navier-Stokes Poisson-Nernst-Planck (NS-PNP) system for an electrolyte solution with only two ionic species (one cation and one anion). For completeness, we reported here the NS-PNP equations [1]

$$\nabla \cdot \mathbf{u} = 0 \tag{3}$$

$$\frac{\partial \mathbf{u}}{\partial t} + \mathbf{u} \cdot \nabla \mathbf{u} = -\frac{1}{\rho} \nabla p + \nu \nabla^2 \mathbf{u} + \frac{\rho_e}{\rho} \mathbf{E} \tag{4}$$

$$\frac{\partial n^{\pm}}{\partial t} + \mathbf{u} \cdot \nabla n^{\pm} = -\nabla \cdot \left[ -D^{\pm} \nabla n^{\pm} + n^{\pm} \mu^{\pm} e z^{\pm} \mathbf{E} \right] \tag{5}$$

$$\nabla^2 \Phi = -\frac{\rho_e}{\epsilon} \tag{6}$$

where $p$ is the pressure, $n^+$ and $n^-$ the ion number densities, $\Phi$ the electrical potential, $\mathbf{E} = -\nabla\Phi$ the electric field, $\rho$ and $\nu$ the density and the kinematic viscosity of the solvent (both assumed to be constant and homogeneous), $\mu^+$ and $\mu^-$ the mobilities of the ions, $D^+ = \mu^+ k_B T$ and $D^- = \mu^- k_B T$ their diffusion coefficients, $z^+$ and $z^-$ their ionic valences, $e$ the electron charge, $\epsilon = \epsilon_0 \epsilon_e$, with $\epsilon_0$ the vacuum dielectric constant and $\epsilon_e$ the relative permittivity of the solution and $\rho_e = e(|z^+|n^+ - |z^-|n^-)$ the local charge. Poisson equation is solved on the entire domain (fluid plus solid) while the other equations are solved only in the fluid domain. The matching condition for the electrical field between solid and liquid is

$$\epsilon_0 \epsilon_e \mathbf{E_e} \cdot \hat{\mathbf{n}} = \epsilon_0 \epsilon_w \mathbf{E_w} \cdot \hat{\mathbf{n}} + q_w \,, \tag{7}$$

where the subscript $e$ and $w$ denote the electrolyte and the solid wall, $q_w$ indicates the surface charge distribution at the interface and $\hat{\mathbf{n}}$ the normal to the solid-liquid interface pointing towards the liquid [1, 2]. In this work, we used $q_w = -0.016$ C/m$^2$, while the relative dielectric constant are $\epsilon_w = 11.8$ for Si and $\epsilon_w = 9.7$ for $SiN_x$.

The system set-up is sketched in figure S8. Note that, to save computational resources we are imposing a cylindrical symmetry, hence the 2D axial-symmetric system corresponds to a conical pore and not strictly to the actual shape of the pore.

**Pore wall model.** Pore confinement is introduced as an external force that repels the polymer beads when they get close to the pore surface. Also an attractive component mimicking possible adsorbtion at the wall is included. The corresponding potential is defined as follows [13]

$$U_w(\mathbf{r}) = \int_W \phi_w(\mathbf{r} - \mathbf{r}')\, d\mathbf{r}' \tag{8}$$

where $\phi_w$ is a LJ potential, We used $\sigma_w = 5$ nm and we calibrate $\epsilon$ to get $U_w \simeq k_B T$ approximatively at the nominal pore wall, i.e. the one where no slip boundary condition is applied in continuum simulations and to get $U_w \simeq -2k_B T$, as minimum of the wall potential. A sinusoidal perturbation on the scale of the bead distance, $b$, is added to make the polymer experiences also a tangential force along the wall which simulates friction effects.

**Simulation procedure.** To induce a self-entangled conformation of the dsDNA, we generated a random chain conformation inside the pore. In this initial highly compacted conformation, several

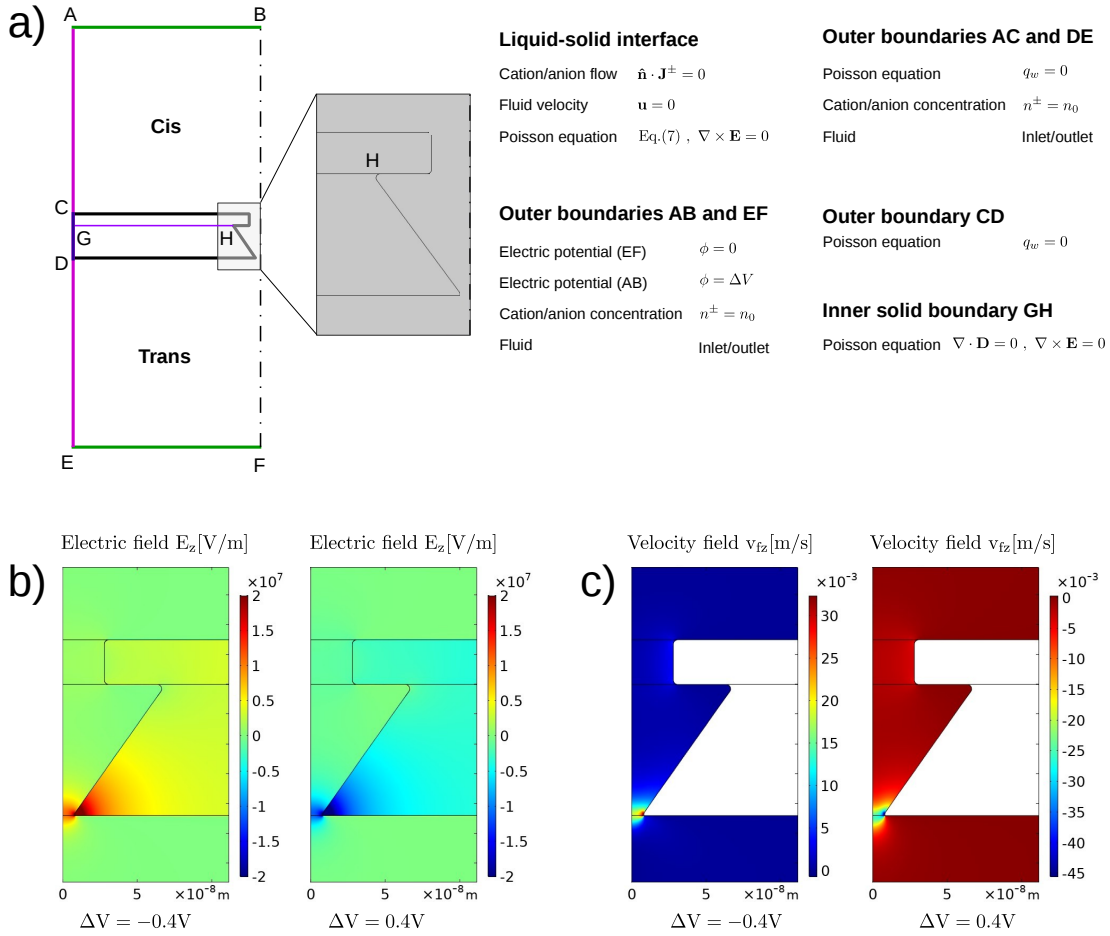


**Figure S8: Continuum simulation set-up.** a) Simulations were run in an 2D axial-symmetric domain. In the solid domain only the Poisson equation is solved while in the liquid domain the entire NS-PNP system is computed. The total size of the simulation in axial direction is 1118 nm while the radial size is 500 nm. Panels b) and c) report the axial component of the electric and of the fluid velocity fields in the pore region for applied voltages $\Delta V = 0.4V$ and $\Delta V = -0.4V$.

overlaps among the beads are present. To avoid strong numerical instabilities, due to the large forces among overlapping beads, the first 0.8 $\mu$s of the simulation was run with shorter range WCA forces (cutoff = 0.95 $\sigma$). Moreover, $\Delta V = 0$, to switch off electrophoresis and electroosmosis, as a consequence, the pore confinement is the only external action on the polymer. This first equilibration allows the polymer to gradually reach a conformation consistent with the exclusion volume of the beads. A second 0.8 $\mu s$ equilibration is run with standard WCA. The final conformation of this second equilibration was used as initial condition for two non-equilibrium simulations, one using the external electrophoretic and electroosmotic actions from a continuum simulation where a voltage

$\Delta V = 0.4\ V$ is applied between the two electrode and the other corresponding to $\Delta V = -0.4\ V$. The simulations were run for $40\,\mu s$ or until the DNA does not exit from the pore (an event that happens only for positive voltages, when electrophoresis is directed from Trans to Cis reservoir). In all the simulations, the temperature was set to $T = 300$ K the persistence length to $\ell_p = 50$ nm. The equilibrium distance between consecutive beads is $b = 4$ nm, while the WCA parameters are $\sigma = 8$ nm and $\epsilon = 10$ kJ mol$^{-1}$. We assigned to each bead a mass of a dsDNA of contour length $b$, i.e. $m = 7.06$ kDa. Concerning the charge of each bead, we selected $q = -5.88$e roughly corresponding to an effective charge of 0.5e on each monomer of the dsDNA. The bead drag coefficient is set to $\gamma = 6\pi\mu b$. For each case, we simulated six different replicas of the described protocol that differs for initial condition and random seed. Since there is a certain degree of arbitrariness in the selection of the coarse-grained parameters, we have performed some consistency checks to verify that the main conclusion of the simulations are not affected by minor changes of the model parameters. For instance, we run additional simulation using $\sigma = 6$ nm instead of $\sigma = 8$ nm or using a more attractive wall (wall potential minimum $V_w = -10k_BT$) or a less attractive wall ($V_w = -0.2k_BT$). The qualitative picture is confirmed, in any case, the polymer remain trapped for $\Delta V < 0$ while is released on the Cis side for $\Delta V > 0$.

## Supplementary references


[1] Henrik Bruus. *Theoretical microfluidics*, volume 18. Oxford university press Oxford, 2008.

[2] Alberto Gubbiotti, Matteo Baldelli, Giovanni Di Muccio, Paolo Malgaretti, Sophie Marbach, and Mauro Chinappi. Electroosmosis in nanopores: computational methods and technological applications. *Advances in Physics: X*, 7(1):2036638, 2022.

[3] Patrick S Doyle and Patrick T Underhill. Brownian dynamics simulations of polymers and soft matter. In *Handbook of materials modeling*, pages 2619–2630. Springer, 2005.

[4] K. Burrage, I. Lenane, and G. Lythe. Numerical methods for second-order stochastic differential equations. *SIAM J. Sci. Comput.*, 29(1):245–264, 2007.

[5] Aleksij Aksimentiev and Klaus Schulten. Imaging $\alpha$-hemolysin with molecular dynamics: ionic conductance, osmotic permeability, and the electrostatic potential map. *Biophysical journal*, 88(6):3745–3761, 2005.

[6] Emma Letizia Bonome, Fabio Cecconi, and Mauro Chinappi. Electroosmotic flow through an $\alpha$-hemolysin nanopore. *Microfluidics and Nanofluidics*, 21(5):96, 2017.

[7] Giovanni Di Muccio, Blasco Morozzo della Rocca, and Mauro Chinappi. Geometrically induced selectivity and unidirectional electroosmosis in uncharged nanopores. *ACS nano*, 2022.

[8] Mauro Chinappi and Fabio Cecconi. Protein sequencing via nanopore based devices: a nanofluidics perspective. *Journal of Physics: Condensed Matter*, 30(20):204002, 2018.

[9] Kherim Willems, Dino Ruić, Florian LR Lucas, Ujjal Barman, Niels Verellen, Johan Hofkens, Giovanni Maglia, and Pol Van Dorpe. Accurate modeling of a biological nanopore with an extended continuum framework. *Nanoscale*, 12(32):16775–16795, 2020.

[10] Mauro Chinappi, Misa Yamaji, Ryuji Kawano, and Fabio Cecconi. Analytical model for particle capture in nanopores elucidates competition among electrophoresis, electroosmosis, and dielectrophoresis. *ACS nano*, 14(11):15816–15828, 2020.

[11] Meni Wanunu, Will Morrison, Yitzhak Rabin, Alexander Y Grosberg, and Amit Meller. Electrostatic focusing of unlabelled dna into nanoscale pores using a salt gradient. *Nature nanotechnology*, 5(2):160–165, 2009.

[12] Mauro Chinappi, Tudor Luchian, and Fabio Cecconi. Nanopore tweezers: Voltage-controlled trapping and releasing of analytes. *Physical Review E*, 92(3):032714, 2015.

[13] M Chinappi, E De Angelis, S Melchionna, CM Casciola, S Succi, and R Piva. Molecular dynamics simulation of ratchet motion in an asymmetric nanochannel. *Physical review letters*, 97(14):144509, 2006.